

## A Numerical Investigation of the Viscous 2-D Cavitating Flow over a Wall-Mounted Fence

B. W. Pearce, P. A. Brandner and J. R. Binns

Australian Maritime College  
University of Tasmania, Launceston, Tasmania 7250, Australia

### Abstract

Two-dimensional flow over a wall-mounted fence with a finite length cavity detaching from the fence is investigated using computational fluid dynamics. The effect of boundary layer thickness to fence height ratio on cavity characteristics, general flow topology and upstream wall pressure distribution is investigated. The viscous analysis was undertaken at a Reynolds number, based on fence height, of 800,000 using a commercial RANS code with the standard  $k-\epsilon$  turbulence model. Results are compared with an inviscid potential flow model to assess the effect of viscosity. A non-linear boundary element method was used to solve the wetted surface/cavity inviscid potential flow problem.

### Introduction

The separated flow over a wall-mounted fence has been of ongoing interest. A basic aspect of this is the effect of the fence on both laminar and turbulent boundary layers [2, 7, 15, 4, 9]. The interest in wall-mounted fence flows within aerodynamics has included the use of spoilers (i.e. fences) as control devices [20, 6] and more recently the use of fixed or oscillating fences for active control of flow separation [12, 17]. The term Gurney flap is in common use in flight and automotive aerodynamics for trailing edge fences fitted to aerofoils and automotive rear wings as lift augmentation devices [18, 16]. There has also been considerable interest in the study of wall-mounted fence flows, in particular of porous fences, in the wind engineering/atmospheric fluid mechanics area with emphasis on the downstream wall pressure distribution and other characteristics of the wake [21, 8].

Within the wealth of published work on wall-mounted fence flows, the particular regime of cavitating flow detaching from a fence has not been addressed in the open literature. The closest work encompassing cavitating wall flow is that associated with backward facing steps [22, 10, 14, 11, 3]. As an attempt to begin to fill in this gap, this brief note reports on a numerical study looking at the effect of a boundary layer on the flow topology and hydrodynamic characteristics of the cavitating flow over a wall-mounted fence. This numerical work is also to be supplemented with a future experimental investigation, to be undertaken in the Cavitation Research Laboratory (CRL) Cavitation Tunnel at the Australian Maritime College (AMC).

This basic study is part of a larger project looking at the hydrodynamic performance of base ventilated hydrofoils where the trailing cavity detaches from geometric discontinuities (forward- and backward-facing steps) on the foil surfaces. Also of related interest is the operation of interceptors, the hydrodynamic term for a trailing edge fence, attached to the transom of high-speed marine craft for trim control and steering applications [19, 5]. In both of these applications the pressure distribution resulting on the wall upstream of the fence is useful as a control/lift force which needs to be both controllable and obtained efficiently. The latter is in respect to the lift developed compared to the increased drag penalty due to the fence protruding into the flow.

To investigate the influence of the boundary layer and its relative thickness on the hydrodynamic performance of a cavitating wall-mounted fence this initial study is focused on the simplest case of a flat-faced fence mounted normal to a flat wall. The arrangement is shown schematically in figure 1. Indicated is a typical cavity shape, detaching from the fence outer edge, with an unsteady re-entrant jet type closure. The fence, of height  $h$ , is protruding into a boundary layer of thickness  $\delta$  (where  $U_\delta = 99\%$  of the freestream velocity,  $U_\infty$ ), and a typical upstream wall pressure distribution is indicated. In addition to a Reynolds number based on fence height  $Re = U_\infty h/v$  (where  $v$  is the kinematic viscosity), this flow is characterised by two other dimensionless parameters. The cavitation number based on vapour pressure,  $\sigma_v = (p_\infty - p_v)/q$ , where  $p_\infty$  is the freestream reference pressure,  $p_v$  is vapour pressure and  $q$  is the freestream dynamic pressure ( $= 1/2\rho U_\infty^2$ ). The reference pressure for the CFD results is defined at  $100h$  upstream of the fence on the domain vertical centreline. The other parameter is the non-dimensional boundary layer thickness,  $\delta/h$ .

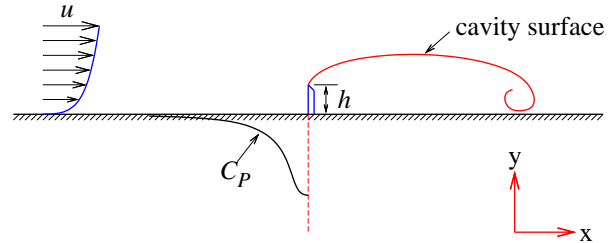


Figure 1: Sketch of a wall mounted fence, height  $h$ , with a vapour/gaseous cavity detaching from the sharp outer edge. The cavity closure is generally unsteady with a re-entrant jet type topography. In a viscous flow the fence will be operating in a boundary layer of thickness,  $\delta$ . Of interest is the pressure distribution along the wall upstream of the fence. The origin of the coordinate system is at the fence/wall junction.

### Numerical Modelling

#### Viscous Flow Analysis with CFD

The commercial computational fluid dynamics (CFD) code, ANSYS-CFX, was used for the viscous numerical analysis presented here. An unsteady two dimensional finite volume method has been used with a structured hexahedral mesh and a high resolution discretisation scheme (third order accurate [1, pp.248-252]). A standard RANSE  $k-\epsilon$  turbulence model was chosen to capture viscous flow features. The interface between vapour and water has been modelled using a volume-of-fluid volume fraction method. The occurrence of vaporisation or condensation is determined by the difference between the absolute pressure and the vapour pressure (here set to be 3574 Pa) and the rate at which it occurs is controlled by a Rayleigh-Plesset (R-P) model as implemented in CFX [1, p.146]. This model uses a simplified and linearised version of the R-P equation

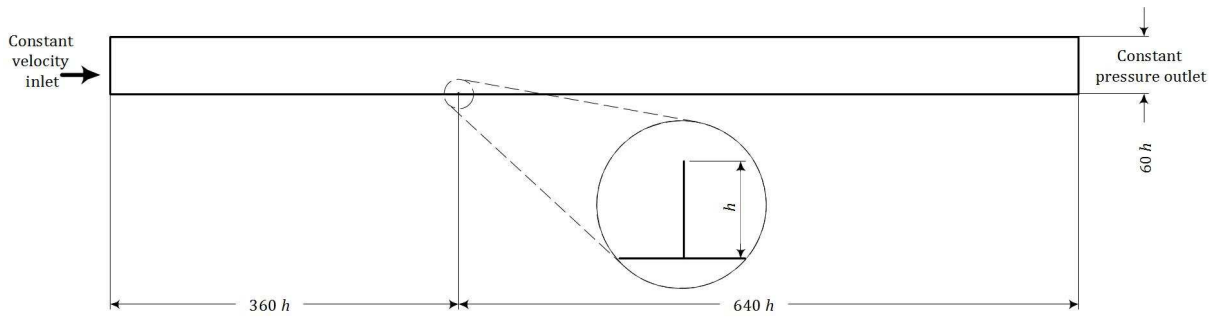


Figure 2: CFD flow domain with the fence attached to the bottom wall and the flow from left to right.

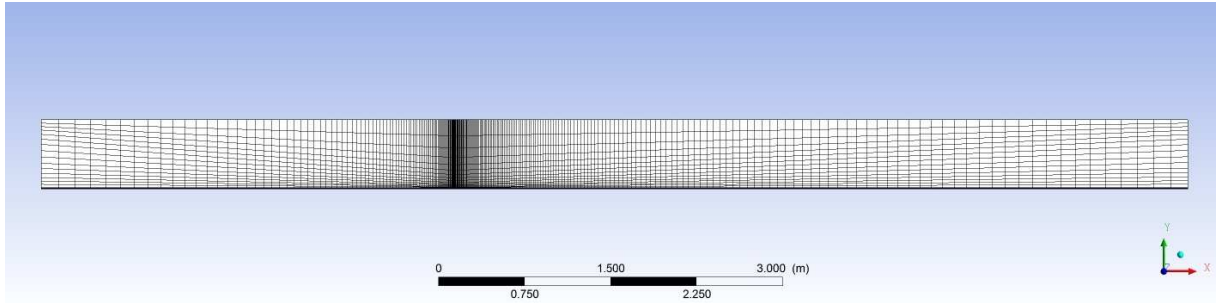


Figure 3: CFD domain discretisation example. A coarse grid is shown to illustrate the grading, in both the x- and y- axes, with local refinement adjacent to the fence (attached to the bottom surface).

applied to an assumed homogeneous bubbly flow from which two equations for vaporisation and condensation respectively are derived. To enable future comparison with experimental data, where the fence will be located on the test section ceiling, a buoyancy force was applied away from the bottom wall in the numerical model.

The computational domain used is shown in figure 2. The fence was modelled within this domain as an infinitely thin wall protruding 10 mm into the flow as shown in the inset. Local refinement off the bottom wall and around the fence was used, which is shown for the coarsest grid used in figure 3.

For the computational domain used, both temporal and spatial grid sensitivity studies were performed. For the spatial variation, grid sizes were varied from 5,750 elements to 1,068,000 elements. From this it was concluded that the length of the cavity formed behind the fence for a grid size of 237,452 elements was within 0.8% of the grid independent solution. Temporal convergence was checked by analysing the spatially converged grid with time steps ranging from 43 ms to 1.5 ms. From this analysis it was concluded that a time step of 2 ms predicted a cavity length within 0.7% of the grid independent solution. As a constant inlet velocity of 8 m/s ( $Re = 8 \times 10^5$ , chosen to enable comparison with future experimental data) has been used throughout, the relationship between spatial convergence and temporal convergence has been assumed to be constant for all runs completed. Using this setup, spread across four partitions on a multi-node cluster (purchased in 2008), runs typically took 30-40 hours to complete.

Cavitation number variation was realised by varying the reference pressure from 8.75 kPa to 25 kPa. Boundary layer thickness variation was achieved by adjusting the wall velocity boundary condition between the upstream domain limit and the fence. boundary layer ( $\delta = 0$ ) was achieved by applying a

wall velocity equal to  $U_\infty$  (i.e. a wall free slip condition) all along the wall up to the fence. Conversely the thickest boundary layer was achieved by setting a zero wall velocity (i.e. a wall zero-slip condition) along the complete upstream length. Intermediate values of boundary layer thickness were then realised by reducing the length of wall subject to the zero-slip condition upstream of the fence, maintaining the fence in the same position in the domain for all cases. In this way numerically stable boundary layers were obtained in the vicinity of the fence, whilst maintaining an easily varied boundary layer thickness. Although a singularity is introduced along the wall due to this mixed boundary condition convergence rates for the various combinations did not vary. The measured boundary layer thickness (at  $x = 0$ ) for each condition was obtained with the fence removed with all other parameters unchanged.

#### Inviscid Flow Analysis with BEM

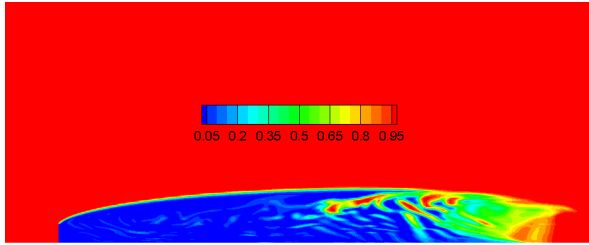
An inviscid analysis was undertaken using a numerical code incorporating a low-order, non-linear, boundary element formulation that has been reported on previously[13]. The method is potential based employing both normal doublets and sources distributed on the foil and cavity surfaces. Cavity shape and surface velocity are unknown for a fixed cavity length and introduce non-linearity to the problem necessitating an iterative solution. Extension of the method to include walls to model the effect of flow confinement on cavitating flows has also been undertaken which is used here to compare with the present CFD data (and with future experimental results).

The boundary element method (BEM) used for this analysis was originally conceived for the analysis of closed bodies (i.e. a solid body with trailing cavity) immersed in a flow. To analyse the cavity flow over a wall mounted fence with this method use was made of the symmetry about the dividing horizontal streamline at the mid-height of a normal flat plate. This together

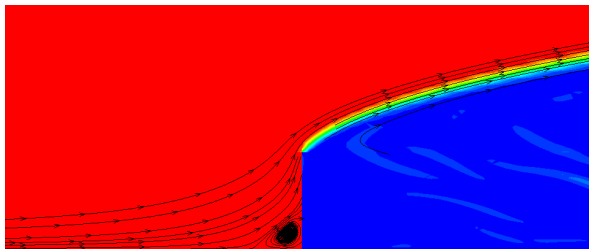
with one half of the plate, with cavity detaching from its outer edge, is then the desired model of a wall mounted fence with cavity. To obtain the pressure distribution along the upstream wall the integral of the velocity influence of each singularity is calculated at each of a suitable number of points. These velocity values were then converted to a pressure via the standard Bernoulli relation.

## Results

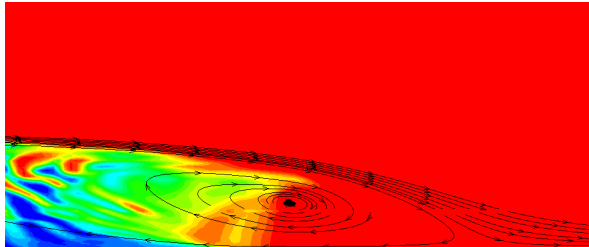
### Cavity shape and flow topology



(a) Fence with attached cavity shown with contours of void fraction.



(b) Streamlines illustrating the upstream flow topology.



(c) Streamlines illustrating the cavity closure topology.

Figure 4: Typical CFD result for cavity flow over a wall-mounted fence ( $\sigma_v = 0.44$  &  $\delta/h = 1.2$ ) with (a) extent of cavity shown as contours of void fraction (0 {100% vapour} to 1.0 {100% liquid}), (b) view of fence with streamlines added showing the separation region in the fence/wall corner, and (c) a view of the cavity closure region showing dividing streamlines either side of stagnation with flow continuing into the wake or reversing forming a re-entrant jet.

Cavity flows generally have an unsteady closure. The cavity length oscillates about a mean position with coherent cycles of vapour structures being shed into the wake and cavity regrowth with re-entrant jet reformation. An unsteady analysis was undertaken to model the physics involved with this process and in figure 4 there is a typical result shown for a cavity shape at an instant in time. The cavity shape is visualized by plotting contours of void fraction. With the potential flow model the cavity has a surface of discontinuity across which the density jumps from that of the water on one side, to the vapour on the other. In a CFD simulation this surface is instead a layer of some finite thickness across which the density gradually reduces till the

change of phase is complete. This behaviour can be seen in the solution shown in figure 4. The closure region is apparent as a mixture of vapour and liquid as fluid is drawn into the cavity by the re-entrant jet. From the streamlines plotted in vicinity of the cavity closure region (figure 4c) the rear stagnation point is found to be further downstream into the mostly liquid region. It was decided to use this point as the extent of the cavity rather than the furthest extent of some arbitrary value of void fraction as this was the point of division of the re-entrant jet flow back into the cavity from that continuing on into the wake.

Of interest also is the flow topology just upstream of the fence when a boundary layer is present. From the streamlines, as plotted in figure 4b, the separated region with reverse flow is present as expected from the results of non-cavitating flows over wall-mounted fences. The separation point on the wall is  $\approx 0.5h$  upstream of the fence and also at  $\approx 0.5h$  up the fence face. This did not vary substantially with the range of  $\delta$  examined ( $0 < \delta/h \leq 3.7$ ).

Figure 5 shows the relationship between cavity length,  $l_c$ , and  $\sigma_v$  for both the inviscid and viscous analyses. The relationship between cavity length and  $\sigma_v$  for potential flow in an infinite domain is a power law ( $l_c = 4.54\sigma_v^{-1.71}$ ) and is shown for reference. Additionally the potential flow relationship for a blocked flow with  $h/D = 60$  is shown for direct comparison with the CFD results (where  $D$  is the separation of the walls confining the flow). The CFD results for the cases of  $\delta/h = 0$  and 1.2 follow the trend of the potential flow blocked relationship. The effect of the boundary layer is to offset the curve  $\delta/h = 0$  downwards, i.e. a shorter cavity is obtained at the same  $\sigma_v$ .

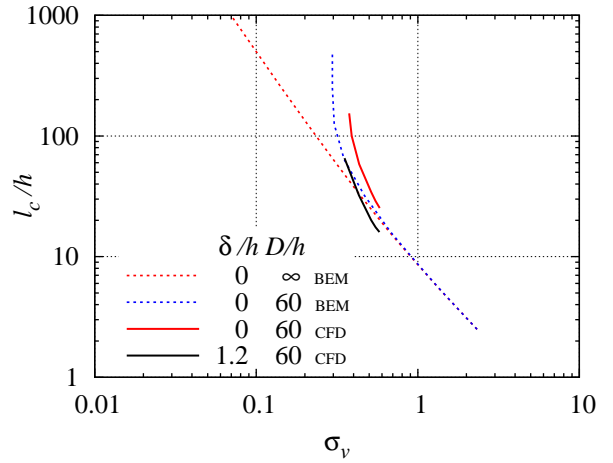


Figure 5: Dependence of cavity length on  $\sigma_v$  for both the viscous and inviscid results. Also plotted is the infinite flow inviscid result for reference.

### Upstream Wall Pressure Distribution

The resultant upstream wall  $C_p$  distribution is shown in figure 6. The pressure coefficient  $C_p$  is defined as  $(p - p_\infty)/q$  with  $p$  the local static pressure. Both the viscous  $\delta/h = 0$  and the inviscid results agree well in the near field out to about  $20h$ . The discrepancy farther upstream is attributable to the presence of solid blockage in the confined CFD flow whereas the BEM result is for an infinite flow. The effect of the presence of a boundary layer is significant. For a  $\delta/h$  of about 1 the maximum  $C_p$  obtained is reduced to about 0.5, i.e. half of the stagnation value obtained at the fence wall junction ( $x = 0$ ) in the absence of a boundary layer. Upon further increase in  $\delta/h$  there is a further reduction of the  $C_p$  extending out to about  $x = 30h$ . Past this

point the two pressure distributions converge and  $C_p \rightarrow 0$  by about  $x = 55h$ . This reduction in magnitude of the wall pressure signature with increase in  $\delta/h$  is expected. The reduced wall pressure reflects the reduced momentum flux due to the presence of a boundary layer, as the flow is deflected from the wall by the presence of the fence.

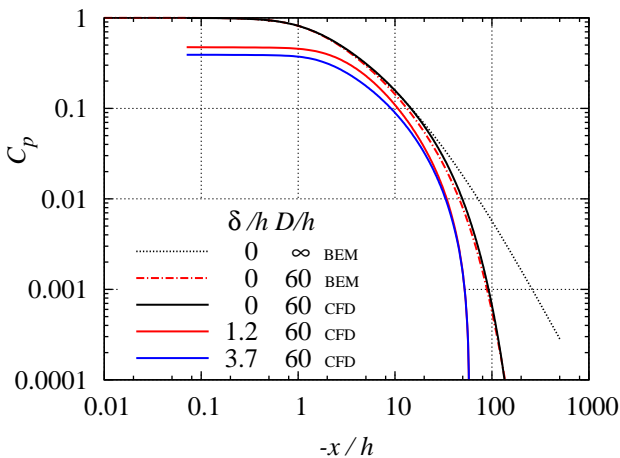


Figure 6: Variation in the upstream wall pressure distribution due to a boundary layer for  $\sigma_v = 0.44$ . The inviscid results (infinite and confined) and viscous result without a boundary layer are shown for comparison.

## Conclusions

The problem of cavity flow over a 2D fence has been numerically investigated using BEM and unsteady CFD methods. In contrast to the BEM prediction the CFD models the re-entrant jet formation and unsteady closure typical of real cavity flows. For the case with a boundary layer a flow separation upstream of the fence is also captured.

The cavity length predicted by the viscous flow analysis follows the trend of the inviscid blocked flow result. The magnitude and extent of the wall pressure distribution is reduced in the viscous cases due to the lower momentum flux in the boundary layer. A more detailed analysis of results covering a greater range of parameters is the subject of ongoing work as well as comparison with experimental results.

## References

- [1] ANSYS, *ANSYS CFX-Solver Theory Guide, Release 12.1*, ANSYS Inc., Canonsburg, USA, 2009.
- [2] Arie, M. and Rouse, H., Experiments on two-dimensional flow over a normal wall, *J. Fluid Mech.*, **1**, 1956, 129–141.
- [3] Brice, R., *Ventilated super-cavitating flow past a backward facing step*, Undergraduate thesis, Australian Maritime College, 2006.
- [4] Durst, F. and Rastogi, A. K., Turbulent flow over two-dimensional fences, in *Turbulent Shear Flows 2*, editors L. Bradbury, F. Durst, B. Launder, F. Schmidt and J. Whitelaw, Springer-Verlag, Berlin, 1980, 218–232.
- [5] Faltinsen, O. M., *Hydrodynamics of high-speed marine vehicles*, Cambridge University Press, Cambridge, Eng., 2005.
- [6] Gerontakos, P. and Lee, T., Particle image velocimetry investigation of flow over unsteady airfoil with trailing-edge strip, *Exp. Fluids*, **44**, 2008, 539–556.
- [7] Good, M. C. and Joubert, P. N., The form drag of two-dimensional bluff-plates immersed in turbulent boundary layers, *J. Fluid Mech.*, **31**, 1968, 547–582.
- [8] Kim, H.-B. and Lee, S.-J., Hole diameter effect on flow characteristics of wake behind porous fences having the same porosity, *Fluid Dyn. Res.*, **28**, 2001, 449–464.
- [9] Kim, H. B. and Lee, S. J., Time-resolved velocity field measurements of separated flow in front of a vertical fence, *Exp. Fluids*, **31**, 2001, 249–257.
- [10] Laali, A. R. and Michel, J. M., Air entrainment in ventilated cavities: case of the fully developed half-cavity, *J. Fluids Engng.*, **106**, 1984, 327–335.
- [11] Maitre, T. and Pellone, C., Numerical modelling of unsteady partial cavities behind a backward facing step, in *4th International Symposium on Cavitation – CAV2001*, editors C. E. Brennen, R. Arndt and S. Ceccio, Cal. Inst. Tech., 2001, Paper B2.002.
- [12] Miau, J. J. and Chen, M. N., Flow structures behind a vertically oscillating fence immersed in a flat-plate turbulent boundary layer, *Exp. Fluids*, **11**, 1991, 118–124.
- [13] Pearce, B. W. and Brandner, P. A., Limitations on 2d super-cavitating hydrofoil performance, in *16th Australasian Fluid Mechanics Conference*, Crown Plaza, Gold Coast, Australia, 2007, 1399–1404.
- [14] Ramamurthy, A. S., Balachandar, R. and Ram, H. S. G., Some characteristics of flow past backward facing steps including cavitation effects, *J. Fluids Engng.*, **113**, 1991, 278–284.
- [15] Ranga Raju, K. G., Loeser, J. and Plate, E. J., Velocity profiles and fence drag for a turbulent boundary layer along smooth and rough flat plates, *J. Fluid Mech.*, **76**, 1976, 383–399.
- [16] Sims-Williams, D. B., White, A. J. and Dominy, R. G., Gurney flap aerodynamic unsteadiness, *Sports Engineering*, **2**, 1999, 221–233.
- [17] Sonnenberger, R., Simultaneous piv- and pressure measurements upstream and downstream of a fence, in *11th Int. Sym. on Appl. of Laser Tech. to Fluid Mech.*, Lisbon, Portugal, 2002, Paper 37.2.
- [18] van Dam, C. P. and Yen, D. T., Gurney flap experiments on airfoils and wings, *J. Aircr.*, **36**, 1999, 484–486.
- [19] Widmark, C., Interceptor steering - an efficient means of providing directional control of waterjet propelled craft, in *Waterjet Propulsion III, International Conference*, RINA, Gothenburg, Sweden, 2001, 1–9.
- [20] Woods, L. C., Theory of aerofoil spoilers, Technical Report 2969, A.R.C., 1953.
- [21] Yaragal, S. C., Ram, H. S. G. and Murthy, K. K., An experimental investigation of flow fields downstream of solid and porous fences, *J. Wind Eng. Ind. Aerodyn.*, **66**, 1997, 127–140.
- [22] Young, A. C. H. and Song, C. C. S., Gravity and free surface effects on a fully cavitating flow, *J. Fluids Engng.*, **97**, 1975, 492–500.